# Production of Copper L X Rays in Heavy-Ion–Atom Collisions*

T. M. Kavanagh, R. C. Der, R. J. Fortner, and M. E. Cunningham

*Lawrence Livermore Laboratory, Livermore, California 94550*

(Received 8 March 1973)

Copper L x-ray production in heavy-ion–atom collisions is discussed. Thick-target x-ray yields and cross sections for x-ray production are presented for copper in the role of both target and projectile. Collision energies were in the range 40 keV to 1.1 MeV and a wide range of collision partners was used. X-ray spectra obtained with a Bragg spectrometer are presented for several of the collision systems. The data, which show strong "level-matching" effects, are interpreted in terms of electron promotion via molecular orbitals, as discussed for asymmetric collisions by Barat and Lichten. Fluorescence yields for the multivacancy states produced in these collisions are discussed, and several solid-target effects are noted.

## I. INTRODUCTION

The creation of inner-shell vacancies in collisions of complex ions and atoms has been studied in several laboratories, and a large body of data has been accumulated.[1] In contrast to the creation of such vacancies by point-charge particles (protons, $\alpha$ particles) cross sections for the heavy-ion case can be very large, approaching the geometric cross sections of the electron orbits for collision velocities much smaller than the orbital velocities of the electrons. We have recently published a summary of measurements in our laboratory of K-shell vacancy production in carbon[2]; the present paper is a similar discussion of an extensive study of L-shell vacancy production in copper. Thick-target yield data and x-ray production cross sections are presented for a wide range of collision systems, with copper in the role of both target and projectile, for collision energies in the range 40 keV to 1.1 MeV. Some of the cross-section data have already been published[3] as an illustration of a marked "level-matching" effect. For the collision velocities used in the present study (ion velocities much smaller than the copper L-electron velocities) the collisions can be considered quasiadiabatic, and interpretation in terms of diabatic molecular orbitals is appropriate.[4]

In addition to the presentation of thick-target yield and cross-section data, results of studies of x-ray spectra are also included. The spectra discussed are relevant to questions of competition for vacancies between the copper L shell and levels of similar binding energy in the collision partner (i.e., in cases of near level matching). The general subject of level matching will be discussed here in more detail than in our earlier Letter.[3] The formulation of Barat and Lichten[5] is used to construct molecular-orbital diagrams for the asymmetric collision systems studied in our experiments, and the level-matching effect is discussed in that context.

We present a discussion of fluorescence-yield effects specific to the copper L-shell case. Whereas in certain cases there can be very large uncertainty in the effective fluorescence yield for the complex distributions of multivacancy states that can be produced in heavy-ion–atom collisions,[6] the copper L-shell case is shown to be relatively insensitive to outer-shell excitation.

Finally, the effects of target-atom recoil, as studied recently by Taulbjerg and Sigmund,[7] are considered and their relevance to the copper data is discussed.

## II. EXPERIMENTAL METHOD

The experimental techniques used have already been discussed extensively.[2,3] All the cross section work was based on thick-target x-ray yields, and the technique for calculating x-ray cross sections from thick-target yields is outlined in Ref. 2. (Possible inadequacies in this approach have been pointed out by Taulbjerg and Sigmund.[7] The effects, in particular, of target-atom recoil will be discussed later.) The x-ray spectra that are presented were obtained using Bragg diffraction techniques described in Refs. 8 and 9; solid targets were also used for these measurements.

Ion beams were obtained from two different machines: High-energy x-ray yield data for carbon, oxygen, neon, and argon ions incident on copper were obtained from a Van de Graaf accelerator, and for the remainder of the data (including the spectral measurements) a 120-kV ion source was used. The ~940-eV copper L x rays were detected in the yield measurements by

a gas-flow proportional counter utilizing a 0.5-mil-thick beryllium or 0.125-mil Mylar window, and a similar detector with an ~90-$\mu g/cm^2$ Formvar window was used in the Bragg spectrometer. A potassium-acid-pthalate (KAP) crystal was used in the Bragg spectrometer as the diffracting element. The spectrometer resolution [full width at half-maximum (FWHM)] was about 35 eV in the vicinity of the copper $L$ x ray.

In the measurements on the 120-kV accelerator, multiply charged ions were used fairly extensively to extend the energy range. (For example, all yield data for copper projectiles were taken using doubly ionized copper. For a given ion kinetic energy, the measured x-ray yields were independent of the charge state of the incident ion, to within the experimental errors.) In order to reduce incident-ion buildup and surface contamination effects all data points in the yield measurements were from short bombardments (a few microcoulombs of incident beam) on a fresh target spot. All target surfaces were initially cleaned with 600-grit paper and washed in alcohol. Absolute yields were, in all cases, obtained by following the heavy-ion bombardments with proton bombardment of copper, and then normalizing

the heavy-ion yield in accordance with previously published absolute-yield data for protons.[10]

## III. EXPERIMENTAL DATA

### A. Thick-Target Yields

Experimental yields of copper $L$ x rays are shown for the many different collision systems in Figs. 1–5. Thick-target yields (x rays emitted per incident ion, assuming isotropic x-ray emission) are plotted as a function of incident-ion energy. Figures 1 and 2 are for copper targets and Figs. 3–5 are for incident copper ions; the collision partner is designated for each curve. Thus in Figs. 1 and 2 the data represent yields of x rays from copper target atoms and the data in Figs. 3–5 are for x-ray emission from copper ions. Standard errors in the thick-target yields are estimated at 15% unless otherwise indicated by error bars in the figures; statistical (counting) errors were usually negligible, and the uncertainties represent estimates of systematic effects.

The yield data shown for the copper targets (Figs. 1 and 2) probably contain some contribution from recoil effects in the target (i.e., x rays are generated in Cu-Cu collisions); this effect can be important for the heavier projectiles, and for $Xe^+$-
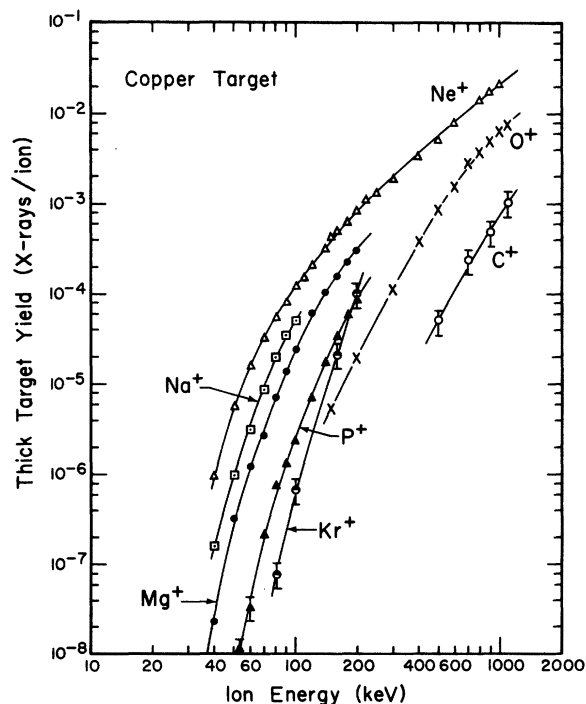


FIG. 1. Thick-target yields of copper $L$ x rays from copper targets bombarded with various heavy ions. Experimental errors are estimated to be ±15% unless otherwise indicated by error bars.
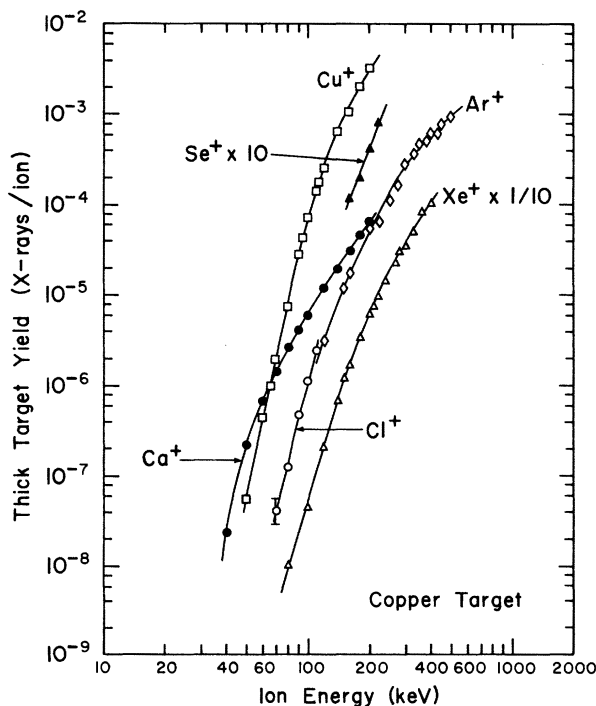


FIG. 2. Thick-target yields of copper $L$ x rays from copper targets bombarded with various heavy ions. Experimental errors are estimated to be ±15%.

Cu may actually account for a major part of the observed yield.[11] This effect may also be important for incident $Kr^+$ and $Se^+$. The experimental yield curves still, however, rigorously designate *thick-target x-ray yields*. These recoil effects of course do not contribute to x-ray yields from the *incident ions*, as in Figs. 3–5.

For certain collision systems (i.e., those located near peaks in level-matching curves—see later discussion) excitation of the collision partner could produce x rays that were not resolved by the proportional counter alone from the $L$ x rays of copper. The problem is most severe when collision partner x rays have energies *slightly* lower than the copper $L$ x rays; in this case the former can dominate the spectra. For cases in which the collision-partner x ray was sufficiently lower in energy than the copper $L$ x ray, beryllium absorbers were used to remove the interfering component. (Successively thicker absorbers were used until the yield curve, normalized to the copper $L$ x-ray yield for protons, became independent of absorber thickness.) For collision systems in which the x-ray energies were more closely matched, corrections to the proportional counter yield data were determined using the Bragg spectrometer.[8] On this basis, for example, a ~30% correction was made to the yield data
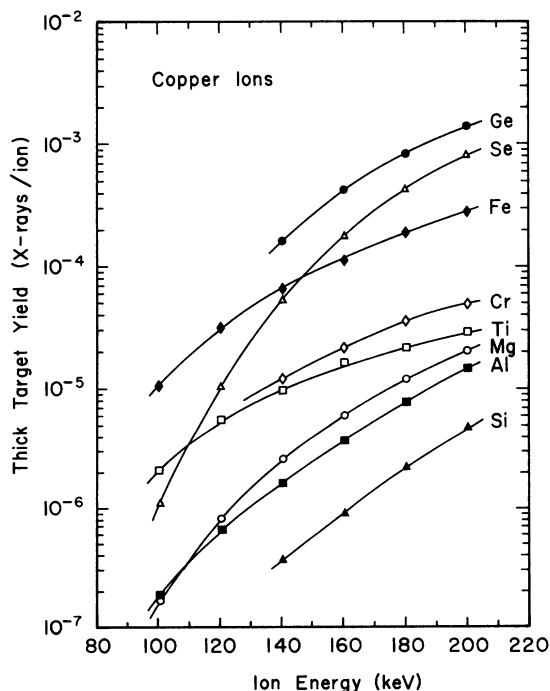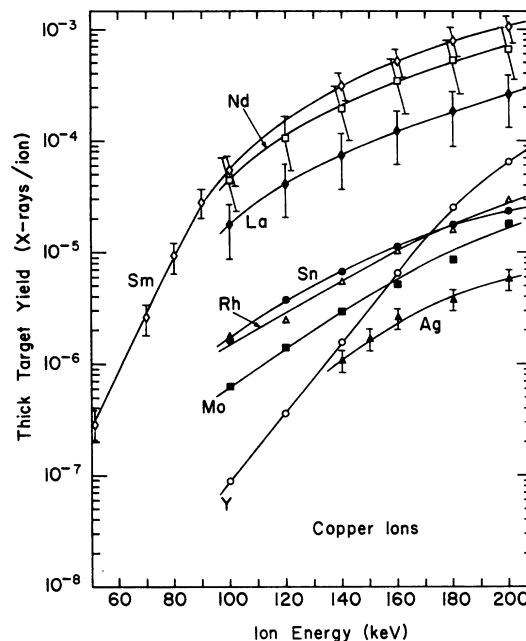


FIG. 4. Thick-target yields of copper $L$ x rays from copper ions incident on various targets. Experimental errors are ±15% unless otherwise indicated by error bars.



FIG. 3. Thick-target yields of copper $L$ x rays from copper ions incident on various targets. Experimental errors are ±15%.
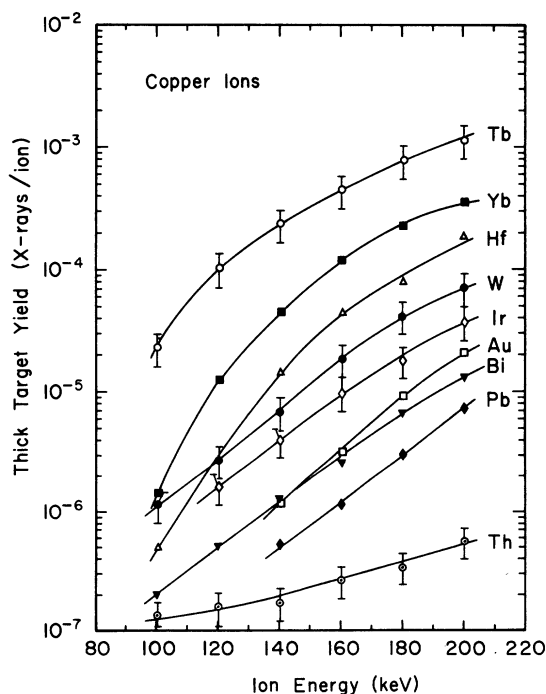


FIG. 5. Thick-target yields of copper $L$ x rays from copper ions incident on various targets. Experimental errors are ±15% unless otherwise indicated by error bars.
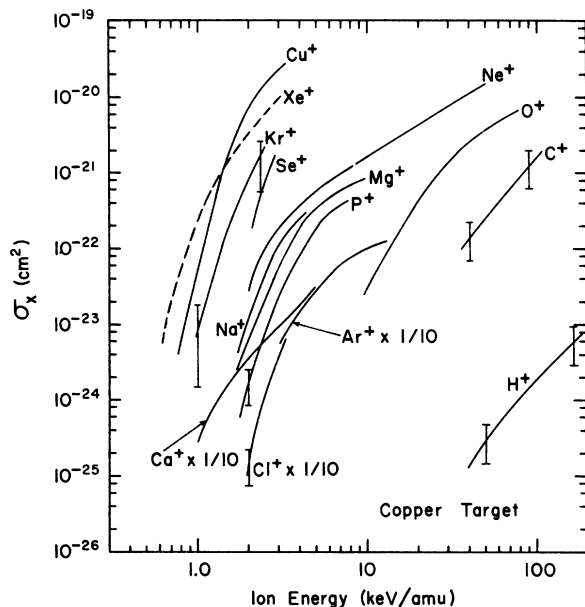
FIG. 6. Cross sections for *L* x-ray production in copper for various heavy ions incident on thick copper targets, as a function of ion energy per amu. The data for incident Xe⁺ and perhaps also Kr⁺ and Se⁺ may be in error due to the recoil effect in solid targets (Refs. 7 and 11). For a discussion of experimental errors, see text.



FIG. 8. Cross sections for *L* x-ray production in copper ions incident on various thick metal targets, as a function of incident ion energy per amu.



FIG. 7. Cross sections for *L* x-ray production in copper ions incident on various thick metal targets, as a function of incident ion energy per amu. For a discussion of experimental errors, see text.
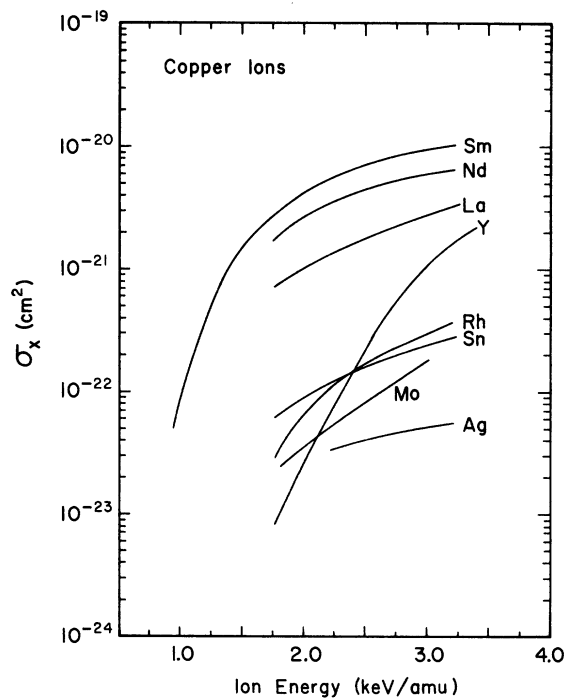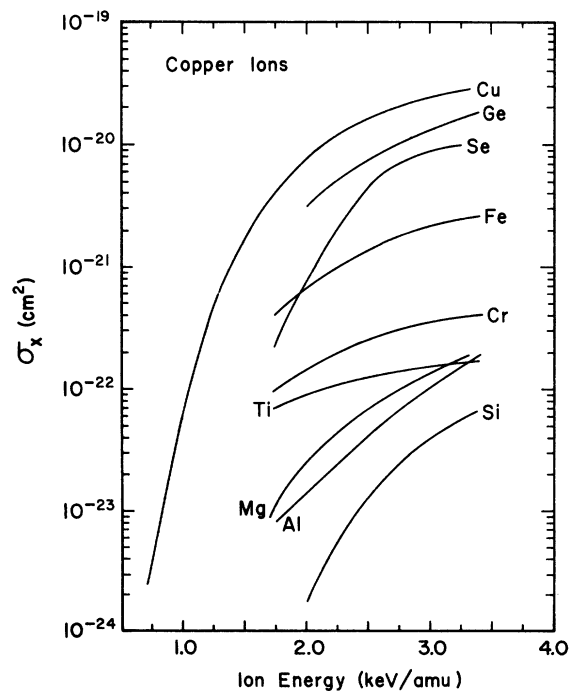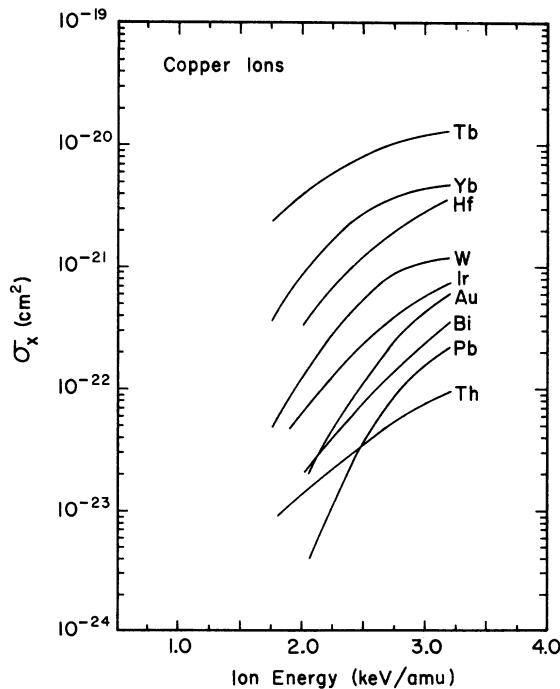


FIG. 9. Cross sections for *L* x-ray production in copper ions incident on various thick metal targets, as a function of incident ion energy per amu.

for neon on copper (Fig. 1) because of unresolved neon $K$ x rays in the proportional counter spectrum, and a similar correction was made for the $Cu^+$-Sm case (Fig. 4) because of samarium $M$ x rays. For cases in which collision partner x rays had energies larger than the copper $L$ x-ray energy, e.g., $Mg^+$-Cu (Fig. 1) and $Cu^+$-Ge (Fig. 3) no interfering x rays were observed. The difficulty in rigorously correcting for these interference effects accounts for some of the atypical experimental errors. The symmetric system $Cu^+$-Cu /of course provides strong overlap of target and projectile x rays; for $Cu^+$-Cu Fig. 2 gives the *total* copper $L$ x-ray yield.

## B. X-Ray Production Cross Sections

Cross sections for x-ray production, calculated from the thick-target yield data are plotted in Figs. 6–9 as a function of ion energy per atomic mass unit (i.e., ion velocity squared). Data for copper targets are summarized in Fig. 6, whereas Figs. 7–9 represent cross sections for x-ray production in the moving copper ion. The cross section for the symmetric $Cu^+$-Cu system is shown in Fig. 6 and, again for comparison in Fig. 7; the curves shown for that case represent the cross section for the *total* interaction, which can produce excitation in either partner. Because of the recoil effect discussed in the previous section, [11] cross section data for $Xe^+$-Cu probably contain large errors, and thus are shown by a dashed line in Fig. 6. The curves in Fig. 6 for $Kr^+$ and $Se^+$ may also contain uncertainty because of target-atom recoil.

In calculating cross sections from thick-target yields the standard formula[12] was used, i.e.,

$$\sigma_x = \frac{dI}{dE} S + \frac{1}{n} \mu I, \tag{1}$$

where $\sigma_x$ is the x-ray production cross section, $I$ is the thick-target yield, $E$ is the ion energy, $S$ is the target stopping cross section for the incident ion, $n$ is the number of target atoms per gram, and $\mu$ is the target absorption coefficient for the copper $L$ x rays. In applying this formula, stopping cross sections were calculated according to the theory of Lindhard et al.[13] and Firsov,[14] for the nuclear and electronic components, respectively. X-ray absorption coefficients were obtained from extrapolations of tabulations of McMaster et al.[15] (The target absorption corrections were, in general, quite small). In an attempt to remove *some* of the subjectivity from the data analysis (in particular the determination of $dI/dE$), the cross-section calculation involved computer smoothing of the yield data. We stress that near

the ends of a yield curve, and in cases where yield data show considerable scatter (due, for example, to low counting rates), the determination of $dI/dE$ could involve considerable uncertainty, and this uncertainty is reflected in the final calculated cross sections. Estimated standard errors for portions of the cross section curves not too near the high- and low-energy extremes are approximately 30%, unless otherwise indicated. (In Fig. 6, error bars on both ends of a curve indicate the estimated uncertainty over the whole energy range; error bars at the low-energy end, as for $P^+$ and $Cl^+$ indicate atypical uncertainty at low energy only. For clarity, error bars are not shown for the data in Figs. 7–9 for incident copper ions. Midrange errors for these curves are indicated in Fig. 15, and uncertainties are larger near the ends of the rather limited energy ranges.) The error estimates do not include uncertainties in calculated stopping cross sections or uncertainties due to target-atom recoil. The curve shown in Fig. 6 for incident protons is from Khan et al.[10]
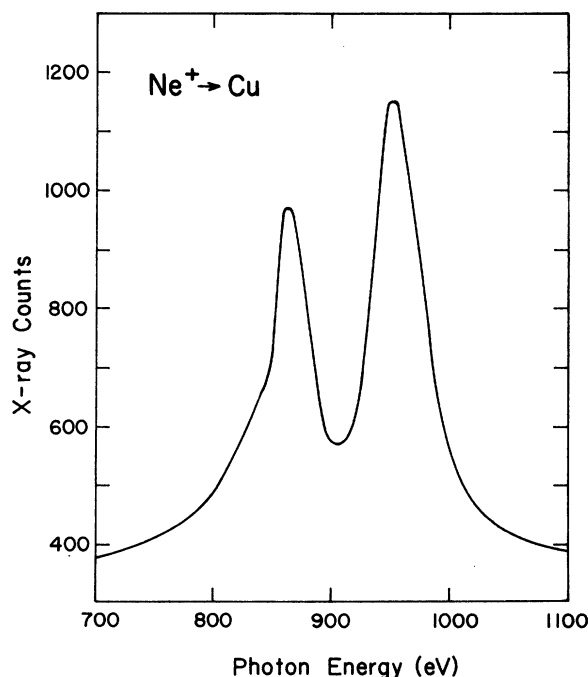


FIG. 10. Experimental x-ray spectrum for a copper target bombarded by 100-keV $Ne^+$ ions. The lower-energy peak represents neon $K$ x rays and the higher-energy peak represents copper $L$ x rays. The curves shown were drawn freehand through about 100 data points; statistical scatter in the original data can be estimated from the vertical scales, which represent total counts per data point.

X-ray production cross-section data like those presented here are of less fundamental relevance in a study of collision phenomena than are cross sections for vacancy production. The two quantities are, of course, related through the fluorescence yield. That is,

$$\sigma_x = \sigma_I \, \omega, \tag{2}$$

where $\omega$ is the fluorescence yield for the shell in question, and $\sigma_I$ represents the cross section for vacancy production. It is now fairly widely recognized that the conversion described by Eq. (2) must be used with caution in heavy-ion interactions, since the creation of multivacancy states in these collisions can profoundly affect fluorescence yields (see, for example, Ref. 6). For this reason, we have chosen to show plots of $\sigma_x$ only. We will show below, however, that normal atomic values for $\omega_L$ probably apply to the data given here, and $\sigma_I$ values could thus be fairly reliably obtained from the plotted $\sigma_x$ data using an ordinary fluorescence-yield value (e.g., 0.0056).[16]

### C. X-Ray Spectra

Data on x-ray spectra, for photon energies in the vicinity of the copper $L$ x ray, are presented in Figs. 10–12. Data were taken with the Bragg spectrometer. Figure 10, for the Ne$^+$-Cu collision, represents a case where collision partner $K$ x rays can interfere with the low resolution (proportional counter) studies of copper $L$ x rays. The spectra in Fig. 11 are for a region of target atomic numbers $(Z_2)$ for which the target-atom $L$ x rays can interfere with $L$ x rays from incident copper ions, and Fig. 12 shows similar data
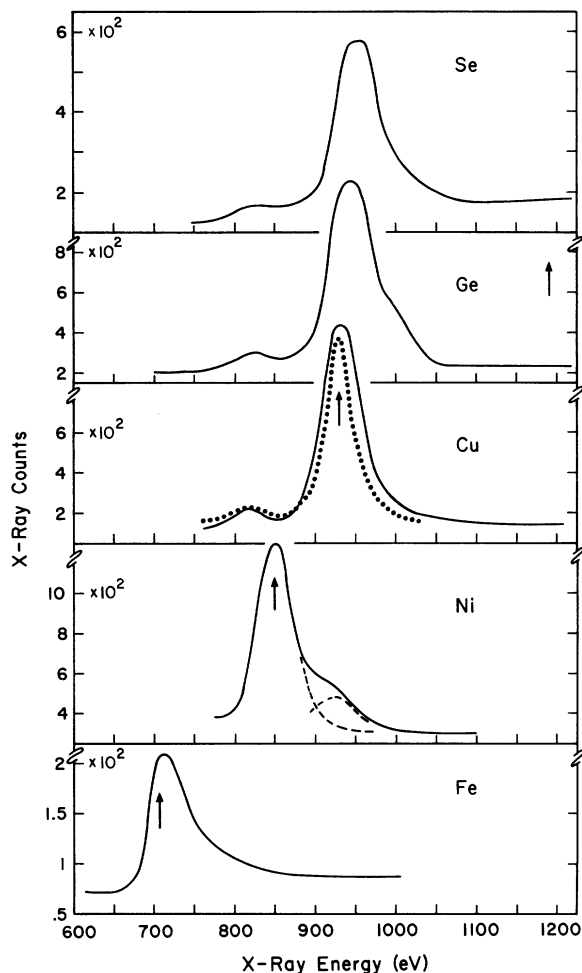
FIG. 11. Experimental x-ray spectra for Fe, Ni, Cu, Ge, and Se targets bombarded by 200-keV Cu$^{++}$ ions. The curves shown were drawn freehand through ~100 data points as in Fig. 10. The arrows shown in the figure give the normal $L\alpha$ x-ray energies for the respective targets; note that for Ge $(Z_2 = 32)$ the $L\alpha$ energy is at the extreme right and for Se $(Z_2 = 34)$ it is off-scale to the right (at 1379 eV). The dotted curve for $Z_2 = 29$ is a spectrum of copper $L$ x rays obtained by bombarding copper with 100-keV protons; the major peak is the $L\alpha,\beta$ component and the lower energy peak is the $Ll,\eta$ component.
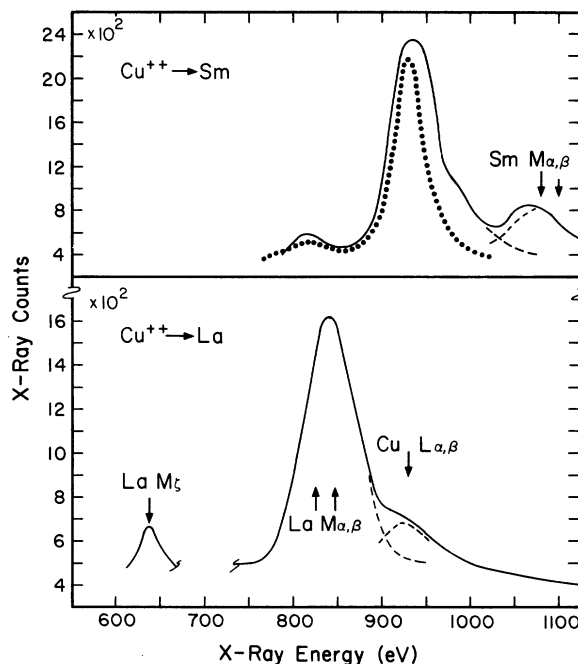
FIG. 12. Experimental x-ray spectra for La and Sm targets bombarded by 200-keV Cu$^{++}$ ions. The curves shown were drawn freehand through ~100 data points as in Figs. 10 and 11. The dotted curve in the upper figure is a copper $L$ x-ray spectrum obtained from 100-keV proton bombardment of copper.

for cases involving competition between the copper $L$ shell and the collision partner $M$ shell. In Figs. 11 and 12 spectra of copper $L$ x rays obtained from proton bombardment of copper are shown for comparison. All spectra were from thick targets, and they have not been corrected for variation of spectrometer efficiency with photon energy, or for target self-absorption.

## IV. DISCUSSION

### A. Cross Sections

The cross-section data illustrate two important features of the heavy ion-atom interaction: cross sections are much larger, for low collision velocities, than is the case for incident protons and $\alpha$ particles, and the cross sections depend very strongly on the relative electron binding energies for the two collision partners.

The first point is illustrated in Fig. 13, in which we have plotted most of the data from Fig. 6 in terms of reduced variables such as those used by Garcia[17] in fitting proton and $\alpha$-particle data to the binary encounter theory. (Note that the abscissa $E/\lambda u$ is equal to the square of the ratio of ion velocity to the copper $L$-electron velocity, and thus can be taken as an indicator of the degree of adiabaticity of the interaction.) Whereas the binary encounter theory quite successfully collapses experimental data for light ions onto the theoretical curve shown in the figure,[17] it is clearly in-

adequate for the heavy-ion case. In Fig. 13 we have used the actual projectile $Z$ value for $Z_1$; the more correct use of a screened nuclear charge would increase the discrepancy between the data and the binary encounter curve.

The dependence of the x-ray cross sections on relative electron binding energies is shown in Figs. 14 and 15 for the cases in which copper serves as target and as projectile, respectively. Except for a factor of 3.2 upward adjustment in Fig. 15 of the data point for $Z_2 = 57$, these curves are the same as those given in Ref. 3. X-ray production cross sections are plotted as a function of the atomic number of the collision partner, for several collision velocities in Fig. 14, and for 2.5 keV per amu in Fig. 15. Fluctuations as large as a factor $10^3$ are evident. The dashed curves in the figures indicate electron binding energies, and the cross sections have peak values for those collision systems in which there is a matching of the copper $L$-shell binding energies with certain binding energies in the collision partner. This is the so-called level-matching effect, first observed by Specht[18] and previously discussed by Kavanagh et al.,[3] Cairns and co-workers[19] and by Saris.[20] In the present work, Fig. 14 shows that the amplitude of the fluctuations decreases with increasing velocity; a similar effect was observed by Specht[18] and by Saris.[20] Saris also observed that the level-matching peaks for argon move to larger $Z$ values with increasing bombarding energy;
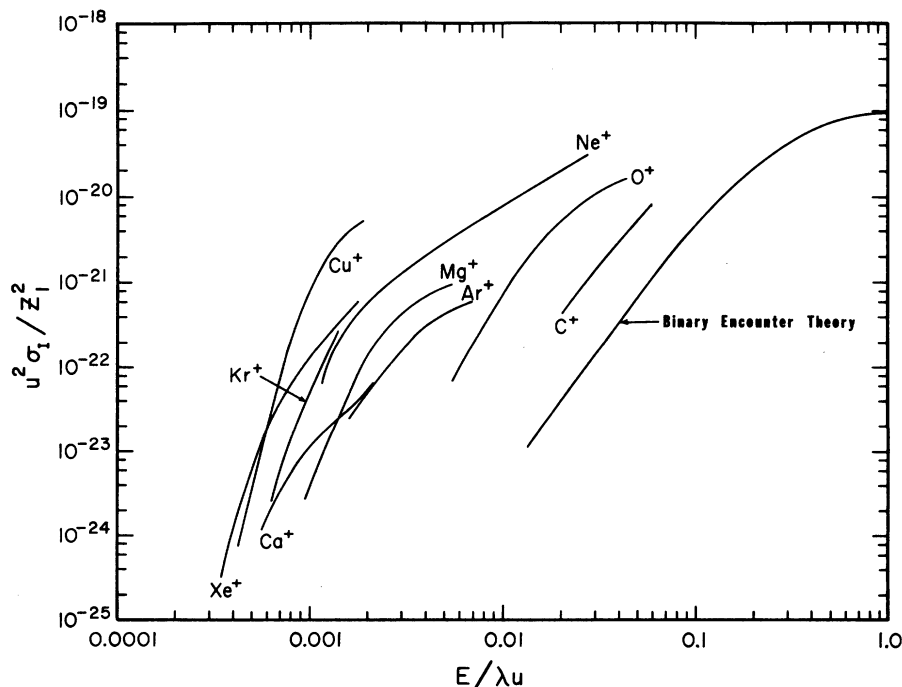


FIG. 13. Cross sections for copper $L$-shell excitation plotted in terms of the reduced parameters used in the binary encounter theory (Ref. 17). $E$ is the incident-ion kinetic energy, $u$ is the binding energy of the relevant electron and $\lambda$ is the ratio of the ion mass to the electron mass. In the ordinate, $\sigma_I$ is the cross section for vacancy production obtained by assuming a constant fluorescence yield value of 0.0056, (Ref. 16) and $Z_1$ is the atomic number of the incident ion.

while no such effect is evident in the copper data in Fig. 14, plots as in Fig. 15 for incident copper ions of different velocities would show such a shift (see Figs. 7–9 in which cross-section curves are steeper for target $Z$ values on the high-$Z$ sides of the level-matching peaks).

Comparisons of the copper data with the *gas-target* data of Saris[20] (as above) should be made with caution, since multiple excitation effects in ions moving in solid targets can influence x-ray production in a variety of ways.[21−23] In connection with our copper measurements, we have already pointed out[3] a lack of reciprocity in the role of target and projectile: in regions of data overlap, the curve in Fig. 15 for copper projectiles appears to be shifted to the right by one or two units in $Z$ relative to the data in Fig. 14. This was attributed[3] to relative *increases* in binding energies in the *projectile* owing to multiple outershell excitations. Target-atom recoil[7] can also lead to differences in the curves of Figs. 14 and 15; this mechanism for x-ray production is not operative for the cases in Fig. 15, but can be important in studies of x rays from target atoms. The data point for Xe ($Z_1 = 54$) in Fig. 14 may be too high by a large factor,[11] and points for Kr$^+$ and Se$^+$ may also be in error.[11] In Figs. 14 and 15,

points for Cu$^{++}$ → Cu were obtained by assuming that the total cross section for this system contains equal contributions from target and projectile.

### B. X-Ray Spectra

The spectrum in Fig. 10 represents a collision system in the left-hand peak in Fig. 14, i.e., corresponding to the region of $K$ shell-$L$ shell matching; the spectra in Figs. 11 and 12 correspond to systems in the $L$-$L$ and $L$-$M$ matching peaks in Fig. 15. Except for the Ne$^+$-Cu case (Fig. 10), which shows a strong solid-state effect, the spectra all show that in these regions of near-matching levels, vacancies are produced predominantly in the level with lowest binding energy. This was mentioned in our earlier paper[3] and is in agreement with related observations in inelastic scattering experiments.[24]

We first discuss the data in Fig. 11. For Cu$^{++}$-Fe, fairly far down the low-$Z$ side of the $L$-$L$ level-matching peak, iron $L$ x rays overwhelmingly dominate the spectrum. To within the rather poor statistical accuracy in the vicinity of $h\nu \sim$ 930 eV there is no indication of a copper $L$ x ray. Thus in Fig. 15, the point for the Cu$^{++}$-Fe system represents minority events. For Cu$^{++}$-Se and Cu$^{++}$-Ge, on the other hand, on the high-$Z$ side of the level-matching peak, only copper $L$ x rays are observed. Note that in these cases the copper peak is broadened toward higher energy and shows evidence of an additional component on the high-energy side of the main peak. These effects are due to multiple excitation of the copper ion: the
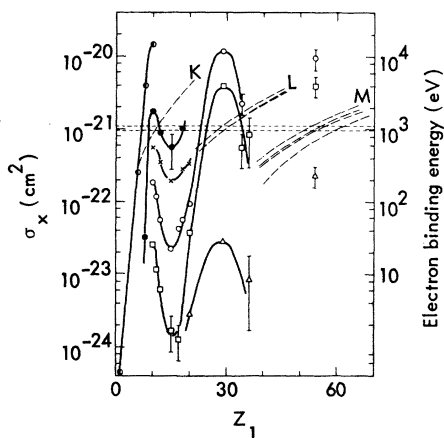


FIG. 14. Cross sections for copper $L$ x-ray production (left-hand scale) in a thick copper target as a function of the atomic number of the incident ion, for different fixed ion energies per atomic mass unit (i.e., fixed ion velocities): triangles, 1.0 keV/amu; squares, 2.0 keV/amu; open circles, 3.0 keV/amu; crosses, 5.0 keV/amu; crossed circles, 10 keV/amu; and half-filled circles, 50 keV/amu. The dashed lines represent ground-state electron binding energies (right-hand scale): The horizontal dashed lines represent copper $L$-shell binding energies, and the dashed curves show electron binding energies for the incident ions as a function of their atomic number. The data points for Xe ($Z_1 = 54$) may be too high due to the recoil effect discussed by Taulbjerg and Sigmund (Ref. 7).



FIG. 15. Cross sections for copper $L$ x-ray production (left-hand scale) in incident copper ions striking solid metal targets, as a function of the atomic number of the target, for a fixed ion energy of 160 keV (2.5 keV/amu). The dashed lines represent ground-state electron binding energies (right-hand scale): The horizontal dashed lines represent copper $L$-shell binding energies, and the dashed curves show target-atom binding energies as a function of target atomic number.

broadening of the major peak is attributed to creation, simultaneous with $L$-shell ionization, of several $M$-shell vacancies, and the high-energy hump probably represents x rays from configurations with double $L$-shell vacancies, i.e., $L$ hypersatellites. (Such multiple excitation occurs with high probability in heavy-ion–atom collisions,[1] and multiple effects are further enhanced by the multiple collisions experienced by the copper ions moving in solid targets.)

The spectrum for $Cu^{++} \rightarrow Cu$ in Fig. 11 shows copper $L$ x rays with less broadening than in the Ge and Se cases, and with no evidence of the higher-energy component. This is consistent with the production of vacancies in $both$ collision partners: The broadening effect seen for $Cu^{++}$-Ge and $Cu^{++}$-Se, and due to multiple collisions of the copper ion in the solid, would be diluted by the presence of x rays from target atoms, and double $L$-shell vacancy production in close collisions is less likely because in a symmetric collision $L$ vacancies are distributed between the two partners. (See molecular orbitals discussion in Sec. IV C.) The near-matching $Cu^{++}$-Ni system probably yields copper $L$ x rays (see the high-energy component in the spectrum) but the spectrum is again dominated by x rays from the lower-$Z$ partner. Note that copper x rays would not be distinguishable, in this case, from $L$-shell hypersatellites of nickel; these double $L$-vacancy contributions, discussed above for the $Cu^{++}$-Ge and $Cu^{++}$-Se cases, probably also account for

the high-energy tail in the iron spectrum.

The spectra in Fig. 12 illustrate cases on either side of the $L$-$M$ match, where (as will be seen in Sec. IV C) the important interaction is between the $L_{II, III}$ and $M_{IV, V}$ subshells. The $Cu^{++}$-Sm system lies just on the high-$Z$ side of the match, and, as expected, x rays from the moving copper ion predominate. The fact that Sm $M$ x rays are observed reflects the relatively small level mismatch. Note that the copper x rays show a breadth and structure similar to that seen for $projectile$ x rays in Figs. 11. In the $Cu^{++}$-La spectrum, representing a system on the low-$Z$ side of the $L$-$M$ match, lanthanum $M$ x rays strongly predominate, with a high-energy component that probably represents copper $L$ x rays; as in the $Cu^{++}$-Ni case, this high-energy structure would also contain any contribution from double $L$-shell vacancies in the target atoms.

The spectrum for $Ne^{+}$-Cu in Fig. 10 is in disagreement with the simple systematics discussed above, i.e., the neon $K$ x rays do not dominate the spectrum. This is a solid-target effect, and we have discussed it previously for the $Ne^{+}$-Cu system[25] and for Ar-C collisions.[22] Outer-shell stripping of the neon ion moving through the solid target can sufficiently increase the neon $K$-shell binding energy so that it $exceeds$ the copper $L$-shell energy. This then leads to creation of copper $L$ vacancies, in accordance with the previously discussed systematics. Such a reversal of level order is expected to occur for neon ions with
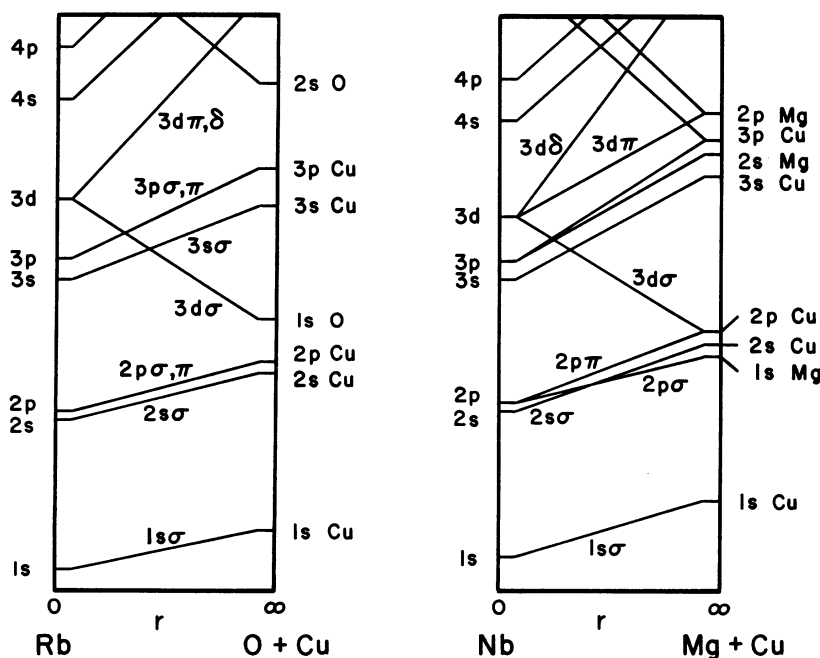


FIG. 16. Correlation diagrams for the collision systems O + Cu and Mg + Cu. The diagram represents electronic energies as a function of internuclear distance $r$; for large $r$ the levels shown are atomic levels of the collision partners, and for small $r$ the energy levels are the atomic levels of the combined atoms. These collision systems bracket the $K$-$L$ level match.

three or more outer-shell vacancies.[26] These
outer-shell effects cause only a small shift in the
energies of the neon *K* x rays, because the neon
$1s$ and $2p$ energies *both* increase rapidly with the
degree of ionization.[26]

### C. Molecular-Orbitals Interpretation

Data of the kind reported here have been widely
interpreted in terms of the electron promotion
model of Fano and Lichten.[4] The large cross
sections, for collision velocities smaller than the
velocities of the electrons being excited, are a
consequence of electron promotion via crossings
of levels of the quasimolecule formed during the
collision. The Fano-Lichten model was extended
to the case of asymmetric (heteronuclear) colli-
sions by Barat and Lichten,[5] and the general
features of the copper data[3] have already been
explained by these authors. A brief discussion
of this interpretation will be given here, and for
further detail the reader is referrred to Ref. 5.

In Figs. 16–18 we show level-correlation dia-
grams for six different collision systems involving
copper. Figure 16 indicates the level correla-
tions for O + Cu and Mg + Cu, which are located on
either side of the *K-L* matching peak (see Fig.
14). Figure 17, for Fe + Cu and Se + Cu, illus-
trates systems on either side of the *L-L* match
(Figs. 14, 15). Figure 18 shows correlations for
La + Cu and Hf + Cu, which are on the high- and
low-*Z* sides, respectively, of the *L-M* matching

peak shown in Fig. 15. As discussed by Barat
and Lichten,[5] the correlation diagrams are con-
structed by joining separated-atom levels, in
order of decreasing binding energy, with the
lowest unfilled level in the combined atom that
has the same number of nodes in its radial wave
function [i.e., equal $(n-l-1)$].

The diagrams are seen to change abruptly with
changing collision partner *Z* in the regions of
level matching. On the low-*Z* side of the *K-L*
match (O + Cu) no level-crossing mechanism is
is indicated, and *L*-shell vacancies would, ac-
cording to the diagrams, result only from direct
excitation mechansims.[12,17] On the high side of
the *K-L* match, however, copper $2p$ electrons
can be promoted via the $3d\sigma$ orbital. (This, how-
ever, does require opening of the exit channel by
prior creation of $2p$ vacancies in magnesium or
$3d$ vacancies in copper. Such an effect has been
demonstrated in solid targets by Lutz *et al.*[23])
At the *L-L* match (Fig. 17) copper $2p$ electrons
are switched from the $3d\sigma$ orbital to the $4f\sigma$ or-
bital, which rises very steeply with many level
crossings. Similarly, in Fig. 18, it is seen that
at the *L-M* match, copper $2p$ electrons can begin
to be promoted via the $5g\sigma$ orbital.

The correlation diagrams thus show "swapping"
of level order, with resultant changes in the pro-
motion schemes, that coincide with peaks in the
cross sections for vacancy production. Large
cross sections are assumed to result from elec-
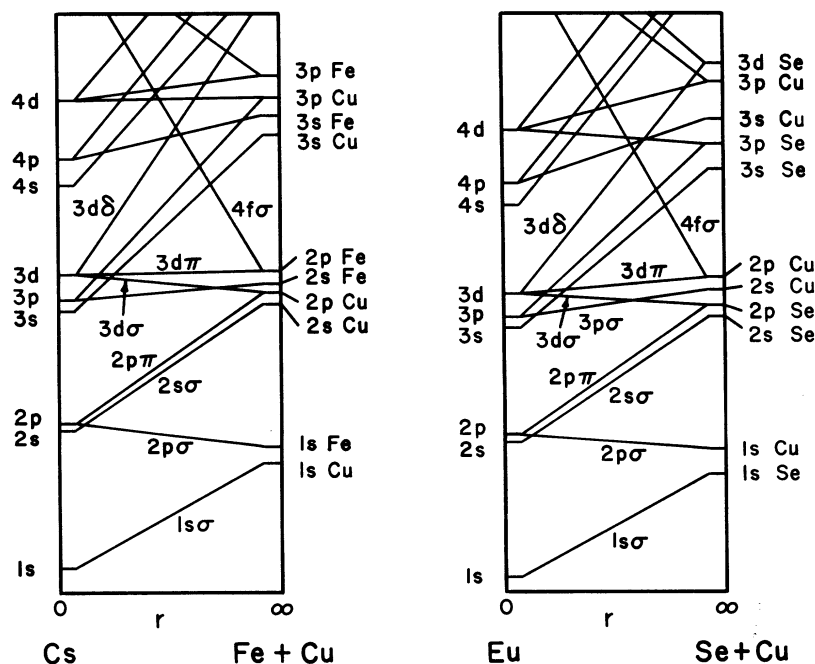tron promotion via steeply rising molecular ener-



FIG. 17. Correlation
diagrams as in Fig. 16,
but for collision systems
on either side of the *L-L*
level match.

gy levels since, in general, these levels can have many crossings with unfilled levels, and they might also couple to the continuum through non-adiabatic terms. [It is important to recognize that steeply rising levels may be effectively very broad during the collision, the width being determined by the product of collision velocity and $dE(r)/dr$.] As discussed by Barat and Lichten, a strict application of the rules of the correlation diagrams would lead to a prediction of discontinuous increases in cross section at a swapping point, rather than the broad peaks that are observed. (See Figs. 14 and 15.) An extreme illustration of this is offered by data on the low-$Z$ side of the $K$-$L$ matching peak: Measured cross sections for copper $L$ excitation by oxygen and carbon ions are much larger than direct scattering theory would predict, yet the correlation diagrams show no copper $2p$ promotion at all. (See Fig. 16.) The cross section decrease on the high-$Z$ sides of the peaks can be understood in terms of decreasing shell radii with increasing $Z$ (i.e., critical $r$ values for promotion are strongly correlated with shell radii),[20] and increasing nuclear repulsion between the collision partners[5]; the nuclear repulsion effect dominates at low energy. The abrupt rise on the low-$Z$ side is probably smeared by level mixing via the uncertainty principle,[5,18] with uncertainties in electron binding energies during the collision reflecting the collision times. (Crucial to this interpretation is the recognition that the interaction length is

small compared to the relevant shell radii.)

Barat and Lichten[5] have attempted an analytical construction of the $L$-$L$ matching peak for copper (Fig. 15), in which they consider the nuclear repulsion effect and the effect of level mixing; the result qualitatively reproduces the structure in the cross-section data.

The spectral data discussed earlier are in excellent accord with the molecular-orbital systematics. Figure 17 would indicate, for example, that for Fe + Cu, vacancy creation in Fe would result from promotion via the steep $4f\sigma$ orbital whereas copper vacancies would result from $3d\sigma$ - $3d\delta$ promotion; this latter path involves a crossing at very small radius with the $3d\delta$ orbital, and the $3d\delta$ orbital may not have a vacancy. For Se + Cu (and Ge + Cu), on the other hand, it is copper $L$-shell vacancies that are created via the $4f\sigma$ orbital, and copper x rays would be expected to dominate, as is observed. Similar arguments follow from Fig. 18 for the La + Cu and Sm + Cu spectra. Note that in the Ne$^+$-Cu case (Fig. 10), the solid-target effect discussed earlier leads, in a significant proportion of the collisions, to a reversal of ordering of the Ne $1s$ and Cu $2p$ levels (see the O - Cu diagram in Fig. 16), with subsequent promotion of copper $2p$ electrons via the $3d\sigma$ orbital. An interesting feature of the spectra in Figs. 11 and 12, which further supports the molecular-orbitals interpretation, is the apparent presence, in all cases except the symmet-
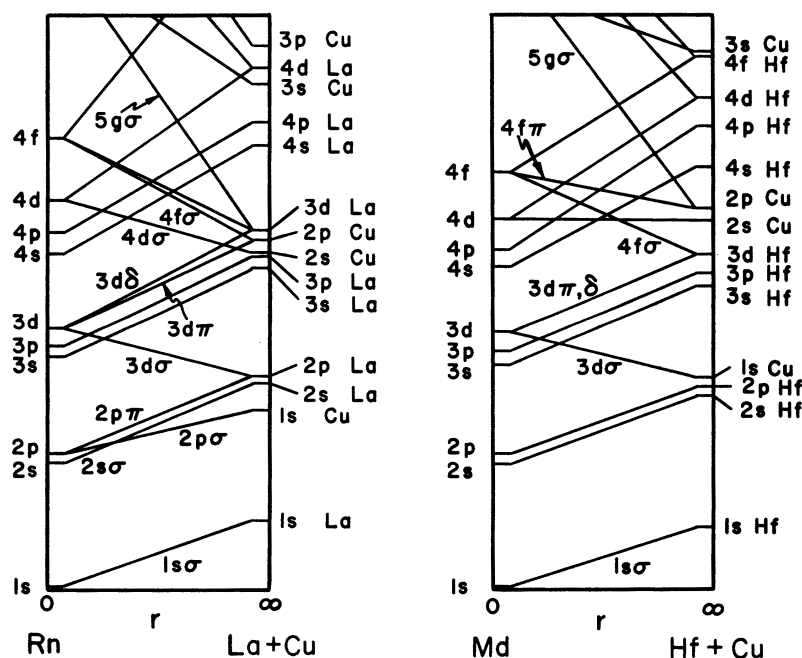


FIG. 18. Correlation diagrams as in Fig. 16, but for collision systems on either side of the $L$-$M$ ($2p$ − $3d$) level match.

ric ($Cu^{++}$-Cu) case, of x rays from double $L$-vacancy states. These $L$ hypersatellites appear for the collision partner of lower $Z$ and thus coincide with promotion via the steeply rising $4f\sigma$ (Fig. 11) or $5g\sigma$ (Fig. 12) orbitals. Since these orbitals contain two electrons, simultaneous promotion of two $L$ electrons is quite probable, with *both* electrons coming from the same partner. In the symmetric case, however, the correlations allow both partners to contribute to $4f\sigma$ promotion and results of scattering experiments (see discussion in Ref. 1) indicate that most likely in cases of double promotion, one electron then comes from each partner. Thus hypersatellites would not be expected in the $Cu^{++}$-Cu spectrum, consistent with observation.

### D. Fluorescence Yields

As has already been discussed in Sec. III B, the multiple-excitation effects that are involved in heavy-ion-atom collisions can lead to large uncertainties in fluorescence-yield values. This can, in turn, lead to large uncertainty in attempts to determine vacancy production cross sections from measured cross sections for x-ray production. Larkins[6] has shown that the effect can be extremely serious in studies of argon $L$-shell excitation. For this reason, we have presented only x-ray production cross sections. Recent calculations by Fortner et al.[27] have shown, however, that the $L$-shell fluorescence yield for copper is relatively insensitive to the moderate amounts of multiple excitation encountered in the present work, and thus normal atomic values[16] are probably appropriate. For completeness, these calculations are discussed briefly below. (For a more complete discussion of the fluorescence-yield question in ion-atom collisions, see Ref. 1.)

The method used for calculating changes in the fluorescence yield has been described by Larkins,[6] and simply involves a correction of the various ground-state Auger and x-ray transition rates for changes in population of outer-shell states. The method assumes that the overlaps of the wave functions are not affected by the defect configuration but that only the populations of the relevant states are changed. In the copper calculations, x-ray transition rates were taken from work of Schofield[28] and Auger rates were extrapolations from work of McGuire.[29]

Results of the calculations for copper are shown in Fig. 19, with argon data from Larkins[6] shown for comparison. Normalized fluorescence yield $\omega/\omega_0$, where $\omega_0$ is the ground-state value, is plotted as a function of the number of $L$-shell vacancies. The outer-shell vacancies were pro-

duced by sequentially removing the most weakly bound electrons. Whereas the $L$-shell fluorescence yield for argon increases rapidly for even a small number of $M$-shell vacancies, the copper value remains essentially constant for up to six $M$-shell vacancies and then decreases until ten $M$-shell vacancies are produced. After ten $M$-shell vacancies, the copper fluorescence yield begins to rise as does that of argon.

The reason for the difference in the two cases can be easily understood. In argon, the principal x-ray transition is the $3s \rightarrow 2p$, i.e., the $Ll$, $\eta$ x-ray lines. The $L\alpha$, $\beta$ x-ray transition ($3d \rightarrow 2p$) does not occur in the ground state since the $3d$ state is not populated. However, in argon the principal Auger transitions involve $3p$ electrons. Now as one starts to remove $3p$ electrons from argon the Auger transition probability drops, yet the x-ray transition probability remains constant and, as a result, the fluorescence yield increases at rapid rate. This is not the case, however, for copper. In copper, the principal x-ray transition is the $L\alpha,\beta$ ($3d \rightarrow 2p$). Likewise, the Auger transition comes principally from transitions involving
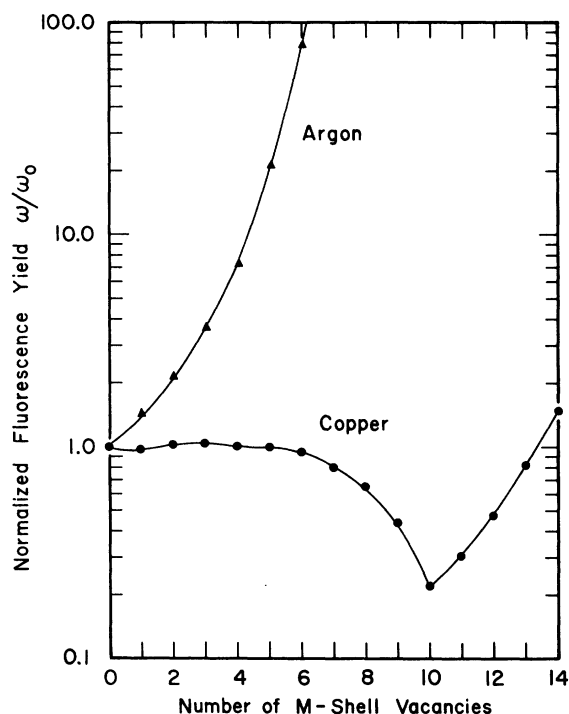


FIG. 19. Normalized $L$-shell fluorescence yields $\omega/\omega_0$ plotted as a function of the number of $M$-shell vacancies for argon and copper. The values for argon are those given by Larkins (Ref. 6) and the copper values were calculated using the radiative transition rates of Scholfield (Ref. 28) and extrapolated Auger rates from McGuire (Ref. 29).

$3d$ electrons. Thus as one removes $3d$ electrons from copper, both the x ray and the Auger transition rates decrease at about the same rate and thus the ratio, the fluorescence yield, is relatively unchanged. This continues to be the case until a large number of $3d$ electrons have been removed. As one continues to remove $3d$ electrons, the Auger transitions involving $3p$ electrons become relatively more important and thus the Auger rate decreases at a smaller rate than the x ray, i.e., the fluorescence yield drops. This continues until all the $3d$ electrons are removed. Once all the $3d$ electrons have been removed, we begin to strip $3p$ electrons and so we have returned to a situation similar to that of argon; the fluorescence yield thus increases with increasing outer shell ionizations.

The fluorescence yields for copper presented in Fig. 19 are for specific atomic configurations where the vacancies have been produced sequentially beginning with the $M_V$ shell. However, an analysis of other atomic configurations indicated that for up to 10 $M$-shell vacancies the fluorescence yield varied by less than 10% provided that all the vacancies were produced in the $M_{IV}$ and $M_V$ shells. Further, the existence of an $M_{III}$, $M_{II}$, or $M_I$ hole has only a small effect on the fluorescence yield; for example, in the case of

six $M$-shell vacancies, even if one of the vacancies was allowed to occur in the $M_{III}$, $M_{II}$, or $M_I$ shell, the calculated fluorescence yields varied only between 0.9 and 1.3 $\omega_0$, depending on the details of the configuration.

Comparison of spectral data (e.g., Figs. 11 and 12) with Hartree-Fock-Slater calculations gives an indication of the degree of $M$-shell excitation accompanying $L$-shell ionization. For copper ions moving in solid targets, and for collision energies $\lesssim 3$ keV/amu, the number of $M$-shell excitations is, on the average, considerably less than eight. Thus fluorescence yield changes would be fairly unimportant. For the case of x rays from target atoms, the spectra indicate even less outer-shell involvement, consistent with expectation. We thus believe that x-ray cross sections from the present work can provide vacancy production cross sections in a straightforward way, with uncertainties that are less than other experimental errors.

## ACKNOWLEDGMENTS

[1] See, for example, J. D. Garcia, R. J. Fortner, and T.M. Kavanagh, Rev. Mod. Phys. 45, 111 (1973); also Proceedings of the International Conference on Inner-Shell Ionization Phenomena, Atlanta, Georgia, 1972, edited by R. W. Fink et al. (USAEC, Oak Ridge, Tenn., 1973).

[2] R. C. Der, R. J. Fortner, T. M. Kavanagh, and J. M. Khan, Phys. Rev. A 4, 556 (1971).

[3] T. M. Kavanagh, M. E. Cunningham, R. C. Der, R. J. Fortner, J. M. Khan, E. J. Zaharis, and J. D. Garcia, Phys. Rev. Lett. 25, 1473 (1970).

[4] U. Fano and W. Lichten, Phys. Rev. Lett. 14, 627 (1965).

[5] M. Barat and W. Lichten, Phys. Rev. A 6, 211 (1972).

[6] F. P. Larkins, J. Phys. B 4, L29 (1971).

[7] K. Taulbjerg and P. Sigmund, Phys. Rev. A 5, 1285 (1971).

[8] R. C. Der, T. A. Boster, M. E. Cunningham, R. J. Fortner, T. M. Kavanagh, and J. M. Khan, Rev. Sci. Instrum. 41, 1797 (1970).

[9] M. E. Cunningham, R. C. Der, R. J. Fortner, T. M. Kavanagh, J. M. Khan, C. B. Layne, E. J. Zaharis, and J. D. Garcia, Phys. Rev. Lett. 24, 931 (1970).

[10] J. M. Khan, D. L. Potter, and R. D. Worley, Phys. Rev. 145, 23 (1966)

[11] K. Taulbjerg, B. Fastrup, and E. Laegsgaard (pri-

vate communication, 1972).

[12] E. Merzbacher and H. W. Lewis, Handbuch der Physik (Springer-Verlag, Berlin, 1958), Vol. 34, p. 166.

[13] J. Lindhard, M. Scharff, and H. E. Schiøtt, K. Dan. Vidensk. Selsk., Mat.-Fys. Medd. 33, No. 14 (1963).

[14] O. B. Firsov, Zh. Eksp. Teor. Fiz. 36, 1517 (1959) [Sov. Phys.-JETP 9, 1076 (1959)].

[15] W. H. McMaster, N. Kerr Del Grande, J. H. Mallet, and J. H. Hubbell, UCRL Report No. 50174, 1969 (unpublished).

[16] R. W. Fink, R. C. Jopson, H. Mark, and C. D. Swift, Rev. Mod. Phys. 38, 513 (1966).

[17] J. D. Garcia, Phys. Rev. A 4, 955 (1971).

[18] H. Specht, Z. Phys. 185, 301 (1965).

[19] J. A. Cairns, D. F. Holloway, and R. S. Nelson, in Proceedings of the International Conference on Atomic Collision Phenomena in Solids, University of Sussex, edited by D. W. Palmer, M. W. Thompson, and P. D. Townsend (North-Holland, Amsterdam, 1969), p. 541.

[20] F. W. Saris, Physica (Utr.) 52, 290 (1971).

[21] F. W. Saris and D. J. Bierman, Phys. Lett. A 35, 199 (1971).

[22] R. C. Der, R. J. Fortner, T. M. Kavanagh, and J. D. Garcia, Phys. Rev. Lett. 27, 1631 (1971).

[23] H. O. Lutz, J. Stein, S. Datz, and C. D. Moak, Phys. Rev. Lett. 28, 8 (1971).

[24] B. Fastrup and G. Hermann, Phys. Rev. Lett. 23, 157

(1969).

[25]R. C. Der, R. J. Fortner, and T. M. Kavanagh, Phys. Lett. 43A, 153 (1973).

[26]F. P. Larkins, J. Phys. B 4, 14 (1971).

[27]R. J. Fortner, R. C. Der, T. M. Kavanagh, and J. D.

Garcia, J. Phys. B 5, L73 (1972).

[28]J. H. Schofield, Phys. Rev. 179, 9 (1969).

[29]E. J. McGuire, Sandia Research Report No. SC-RR-710075 (unpublished).